

# Distinct superconducting states in the pressure-induced metallic structures of the nominal semimetal $\text{Bi}_4\text{Te}_3$

J. R. Jeffries,<sup>1</sup> A. L. Lima Sharma,<sup>2,3</sup> P. A. Sharma,<sup>2</sup> C. D. Spataru,<sup>2</sup> S. K. McCall,<sup>1</sup> J. D. Sugar,<sup>2</sup> S. T. Weir,<sup>1</sup> and Y. K. Vohra<sup>4</sup>

<sup>1</sup>Condensed Matter and Materials Division, Lawrence Livermore National Laboratory, Livermore, California 94550, USA

<sup>2</sup>Materials Physics Department, Sandia National Laboratory, Livermore, California 94551, USA

<sup>3</sup>Department of Physics and Astronomy, San Jose State University, San Jose, California 95192, USA

<sup>4</sup>Department of Physics, University of Alabama at Birmingham, Birmingham, Alabama 35294, USA

(Received 2 August 2011; revised manuscript received 7 September 2011; published 27 September 2011)

The end members, Bi and  $\text{Bi}_2\text{Te}_3$ , of the infinitely adaptive  $(\text{Bi}_2)_m(\text{Bi}_2\text{Te}_3)_n$  series of compounds have not only been revealed to be topological insulators under the appropriate conditions, but have also been shown to be superconductors under pressure, suggesting the potential for bulk superconductor-topological-insulator interfaces and associated quantum computing applications. Herein, we report the pressure-dependent evolution of the structure and electrical transport of the nominal semimetal  $\text{Bi}_4\text{Te}_3$ , a member of the  $(\text{Bi}_2)_m(\text{Bi}_2\text{Te}_3)_n$  series. Under pressure,  $\text{Bi}_4\text{Te}_3$  undergoes several structural phase transformations, ultimately yielding a metallic body-centered-cubic structure exhibiting superconductivity with a maximum  $T_c = 8.4$  K at 16.2 GPa. The occurrence of structure-dependent superconductivity in  $\text{Bi}_4\text{Te}_3$  is remarkably similar to the end members of the  $(\text{Bi}_2)_m(\text{Bi}_2\text{Te}_3)_n$  series, intimating a convergence to high-pressure universal behavior that may expose the subtle variations that lead to the topological insulating and superconducting states in these systems.

DOI: 10.1103/PhysRevB.84.092505

PACS number(s): 64.30.Jk, 74.62.Fj, 74.70.Ad

Recently, superconductor-topological-insulator junctions have been predicted to induce Majorana bound states and the tantalizing prospects for quantum computing.<sup>1–3</sup> While this proximity-induced effect might suffice for quantum computing, the realization of bulk superconductivity in  $\text{Cu}_x\text{Bi}_2\text{Se}_3$  intimates a more controllable route to superconducting-topological-insulator interfaces.<sup>4–6</sup> Furthermore, the observation of superconductivity under pressure in  $\text{Bi}_2\text{Te}_3$  suggests the general feasibility of tuning between topological insulating and superconducting states within the same system.<sup>7</sup>

The nominal semimetal  $\text{Bi}_4\text{Te}_3$  is a member of the trigonal, infinitely adaptive  $(\text{Bi}_2)_m(\text{Bi}_2\text{Te}_3)_n$  series, which is composed of Bi and Te planes assembled from alternating layers of  $\text{Bi}_2$  and  $\text{Bi}_2\text{Te}_3$  building blocks.<sup>8</sup> The end members of this series, Bi and  $\text{Bi}_2\text{Te}_3$ , both display topological insulating behavior, the former through alloying with Sb.<sup>9–11</sup> With applied pressure, Bi and  $\text{Bi}_2\text{Te}_3$  exhibit several different crystal structures<sup>12–14</sup> and distinct superconducting states.<sup>7,15–17</sup> The relationships between these high-pressure superconducting states and the ambient-pressure topologically insulating states are important components to our understanding of the conditions favoring these states. The  $(\text{Bi}_2)_m(\text{Bi}_2\text{Te}_3)_n$  family provides an extensive series that may help to illuminate the subtle differences that create topologically insulating or superconducting states.

Herein, we report a comprehensive structural and electrical transport characterization of semimetal  $\text{Bi}_4\text{Te}_3$  under pressure using diamond anvil cells (DAC). High-pressure x-ray diffraction reveals several structural transformations, culminating in the stabilization of a body-centered-cubic structure at the highest pressures measured. Accompanying these structural changes are modifications in the electronic structure, which manifest a shift from semimetallic behavior at ambient pressure to metallic behavior in the high-pressure phases. Finally, two distinct superconducting states are observed, with the highest-pressure superconducting state exhibiting a

maximum critical temperature comparable to those of Bi and  $\text{Bi}_2\text{Te}_3$  at elevated pressures.

Stoichiometric amounts of elemental Bi and Te (99.99%, Alfa Aesar) were combined in an evacuated quartz tube and melted at 700 °C for 5 days. The melt was then quenched in liquid nitrogen and subsequently annealed at 440 °C for 14 days. X-ray diffraction and electron microscopy confirmed that the samples were single-phase  $\text{Bi}_4\text{Te}_3$  ( $R\bar{3}m$ ) with large ( $\sim 1$  mm) grains. For electrical transport measurements under pressure, single-crystal grains were harvested and loaded into an eight-probe designer DAC<sup>18,19</sup> with steatite as the pressure-transmitting medium and ruby as the pressure calibrant.<sup>20,21</sup> Electrical transport measurements were performed as a function of temperature and magnetic field using the AC Transport option in a Quantum Design PPMS. For structural studies, a conventional DAC was loaded with powdered  $\text{Bi}_4\text{Te}_3$ , fine Cu powder (3–6  $\mu\text{m}$ , Alfa Aesar) as the pressure calibrant, and neon as a pressure-transmitting medium. Room-temperature, angle-dispersive x-ray diffraction experiments were performed at the HPCAT beamline (16 BM-D) of the Advanced Photon Source at Argonne National Laboratory. A  $5 \times 5 \mu\text{m}$ , 30 keV ( $\lambda_{\text{inc}} = 0.4134 \text{ \AA}$ ) incident x-ray beam, calibrated with  $\text{CeO}_2$ , was used. 2D diffraction patterns were collected with a Mar345 image plate, collapsed to 1D intensity versus  $2\Theta$  plots using the program FIT2D,<sup>22</sup> and refined using the programs EXPGUI<sup>23,24</sup> and JADE. *Ab initio* calculations were performed using the QUANTUM ESPRESSO package<sup>25</sup> employing the density functional theory (DFT) formalism with a local density approximation for the exchange correlation potential and including spin-orbit effects.<sup>26</sup>

At ambient pressure,  $\text{Bi}_4\text{Te}_3$  crystallizes in the trigonal  $R\bar{3}m$  space group with  $a = 4.451 \text{ \AA}$  and  $c = 41.888 \text{ \AA}$  (3 formula units per unit cell). Under pressure, the  $R\bar{3}m$  crystal structure compresses relatively easily (bulk modulus  $B_0 \approx 52$  GPa). Near 6.4 GPa, a structural phase transformation occurs (Fig. 1), yielding a slightly stiffer ( $B_0 \approx 77$  GPa) monoclinic unit cell

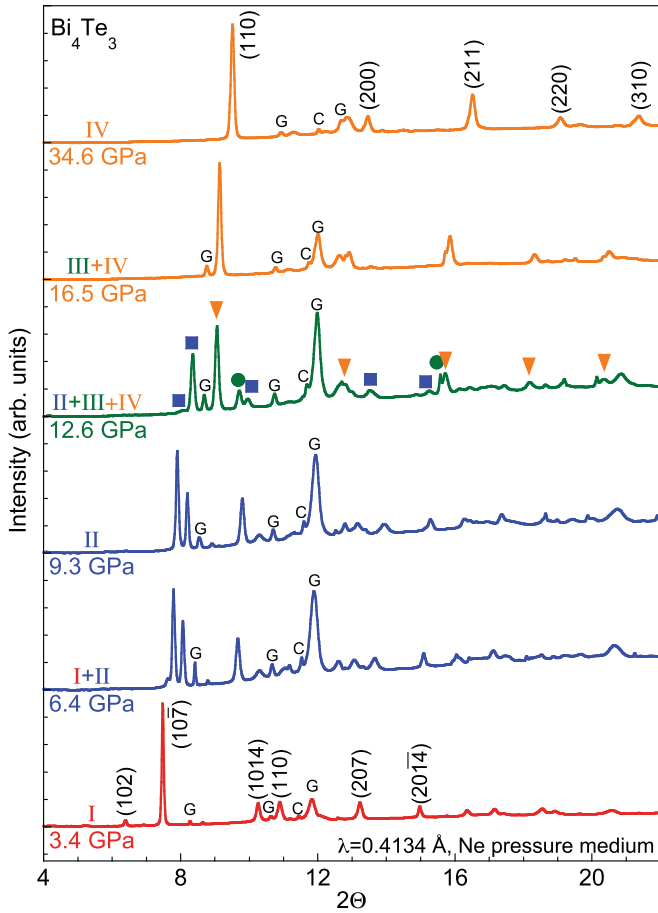


FIG. 1. (Color online) Selected x-ray diffraction patterns of  $\text{Bi}_4\text{Te}_3$  under pressure revealing the different structures:  $\text{Bi}_4\text{Te}_3$ -I ( $R\bar{3}m$ ),  $\text{Bi}_4\text{Te}_3$ -II ( $C2/m$ ),  $\text{Bi}_4\text{Te}_3$ -III, and  $\text{Bi}_4\text{Te}_3$ -IV ( $Im\bar{3}m$ ). Diffraction peaks from the copper pressure marker and gasket are denoted by a “C” and “G,” respectively. Some of the prominent Bragg reflections from the  $\text{Bi}_4\text{Te}_3$ -I and  $\text{Bi}_4\text{Te}_3$ -IV structures are labeled. The pronounced peaks in the multiphase diffraction data at 12.6 GPa are assigned to their respective phases: blue squares,  $\text{Bi}_4\text{Te}_3$ -II; green circles,  $\text{Bi}_4\text{Te}_3$ -III; orange triangles,  $\text{Bi}_4\text{Te}_3$ -IV.

with lattice parameters  $a = 4.3110(34)$ ,  $b = 4.6052(38)$ , and  $c = 6.2641(38)$  Å with  $\beta = 110.22^\circ$ . The reflections from  $\text{Bi}_4\text{Te}_3$ -II index well to a  $C2/m$  space group, yielding a unit cell volume of  $116.70$  Å<sup>3</sup>. Presuming that pressure drives the system into a structure with a lower atomic volume, the unit cell of  $\text{Bi}_4\text{Te}_3$ -II should be constructed from no fewer than 4 atoms; 4- and 5-atom unit cells would imply volume collapses of approximately 3% and 22%, respectively, for the I-II phase transition. We conservatively propose that  $\text{Bi}_4\text{Te}_3$ -II undergoes a moderate volume collapse, suggesting that it is composed of 4 atoms per unit cell. The  $C2/m$  space group and the number of atoms per unit cell for  $\text{Bi}_4\text{Te}_3$  are then identical to those of the high-pressure Bi-II phase.<sup>27</sup> With only 4 atoms per unit cell,  $\text{Bi}_4\text{Te}_3$ -II has fewer than one formula unit per unit cell. In order to maintain the 4:3 Bi:Te ratio in  $\text{Bi}_4\text{Te}_3$ -II, Bi and Te atoms must reside with stoichiometric occupancy at equivalent atomic positions within the unit cell of  $\text{Bi}_4\text{Te}_3$ -II.

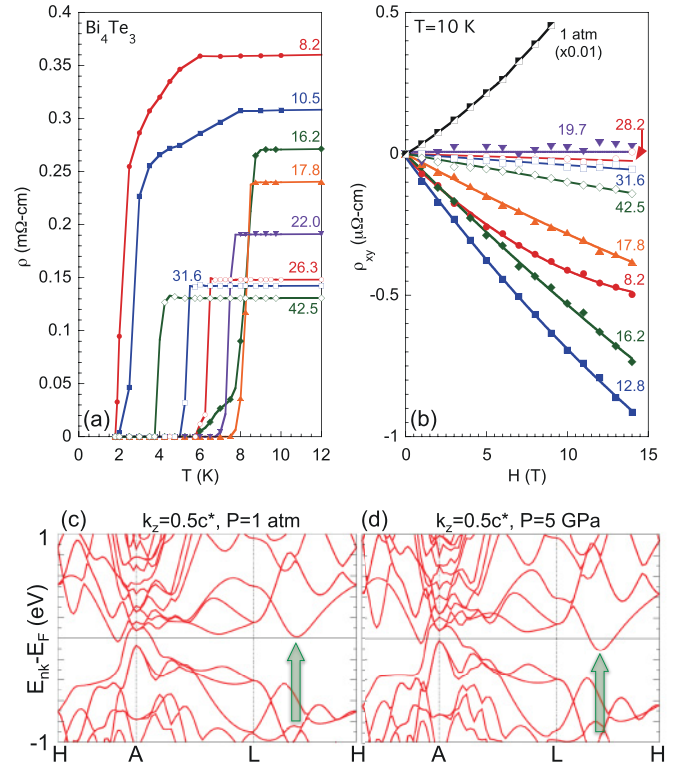


FIG. 2. (Color online) (a) Low-temperature electrical resistivity  $\rho(T)$  for various pressures (in GPa, denoted by text near each curve) revealing the onset and development of superconductivity. (b)  $\rho_{xy}(H)$  for various pressures. (c) LDA band structure calculations confirm the ambient-pressure semimetallic behavior of  $\text{Bi}_4\text{Te}_3$  and (d) reveal the pressure-dependent appearance of an electron-like pocket between the L and H points (green arrows).

Near 11.5 GPa, another phase transformation occurs, producing a multiphase sample where  $\text{Bi}_4\text{Te}_3$ -II coexists with  $\text{Bi}_4\text{Te}_3$ -III and  $\text{Bi}_4\text{Te}_3$ -IV. This multiphase system persists up to approximately 16.5 GPa. Because of its coexistence with other phases, indexing  $\text{Bi}_4\text{Te}_3$ -III was not possible.  $\text{Bi}_4\text{Te}_3$ -IV, on the other hand, appears as a single phase for pressures in excess of 16.5 GPa and is easily indexed to a body-centered-cubic (bcc)  $Im\bar{3}m$  unit cell with  $a = 3.6702(2)$  Å and a volume of  $49.44$  Å<sup>3</sup> ( $B_0 \approx 120$  GPa). With two atoms per unit cell, the bcc  $\text{Bi}_4\text{Te}_3$ -IV phase, like that of  $\text{Bi}_4\text{Te}_3$ -II, contains fewer than one formula unit per unit cell and thus must be described with a similar stoichiometric occupancy of the atomic positions. The high-pressure  $\text{Bi}_4\text{Te}_3$ -IV phase is effectively a disordered bcc alloy of Bi and Te, identical to the high-pressure structures of Bi-V and  $\text{Bi}_2\text{Te}_3$ -IV.<sup>12,14</sup>

Low-temperature  $\rho(T)$  data [Fig. 2(a)] reveal the onset of superconductivity at 8.2 GPa with a  $T_c = 2.1$  K. With further pressure,  $T_c$  increases slightly followed by a discontinuous increase in the transition temperature near 13 GPa. At  $P_c = 16.2$  GPa, the superconducting transition temperature reaches a maximum  $T_c = 8.4$  K, very close to the observed maximum  $T_c$  of Bi (8.4 K) and  $\text{Bi}_2\text{Te}_3$  (9.4 K) under pressure.<sup>15–17</sup> For pressures above 16.2 GPa, the superconducting transition width sharpens, hovering near a width of about 1 K, and  $T_c$  decreases monotonically down to  $T_c = 4.1$  K at 42.5 GPa.

Magnetotransport measurements [Fig. 2(b)] conducted at 10 K show a clear change in the Hall resistivity ( $\rho_{xy}$ ) as a function of pressure. At ambient pressure,  $\text{Bi}_4\text{Te}_3$  is best described as a semimetal due to signatures of ambipolar conduction in Hall effect, Seebeck, and Nernst measurements.<sup>28</sup> While low carrier mobility precludes a quantitative analysis of the ambient-pressure magnetotransport, the presence of electron and hole bands is strongly implied by the qualitative shape of  $\rho_{xy}(H)$ . At 8.2 GPa, the sign of  $\rho_{xy}$  became negative, but the nonlinear field dependence of  $\rho_{xy}$  clearly remains, implying that multiband effects still play a role at this pressure. This multiband behavior yields above 17.8 GPa to a linear field dependence with a minimum slope near 19.7 GPa. At 8.2 GPa, the low-field slope of  $\rho_{xy}$  implies a carrier concentration of order  $10^{21} \text{ cm}^{-3}$ —a borderline value between the expectations for a metal and a semimetal or degenerate semiconductor—while at 31.6 GPa, the  $\rho_{xy}$  data suggest a carrier concentration of order  $10^{23} \text{ cm}^{-3}$ —closer to that of a typical metal.

In order to illuminate the multiband transport in  $\text{Bi}_4\text{Te}_3$ , band structure calculations were performed. These calculations have been restricted to the ambient-pressure ( $R\bar{3}m$ ) phase, because solutions for the site-disordered, high-pressure phases II and IV are intractable with the *ab initio* DFT routine utilized. Figures 2(c) and 2(d) show the electronic dispersions along certain high-symmetry directions in the hexagonal Brillouin zone with  $k_z = 0.5c^*$  ( $c^*$  is the reciprocal lattice vector perpendicular to the Bi/Te layers). At ambient pressure [Fig. 2(c)], a small hole-like section of Fermi surface is visible at zone center (A), a small electron pocket crosses the Fermi level in the A-H direction near zone center, and another electron pocket dips near the Fermi level between the L and H points. This calculation supports the conclusion that both holes and electrons contribute to transport at ambient pressure, but also indicates that any realistic transport model should account for more than two bands. At 5 GPa [Fig. 2(d)], the zone-center hole band increases in size, the small electron pocket near zone center remains nearly unaltered, and the electron pocket between the L and H points crosses the Fermi level. Applied pressure thus causes large electron-like pockets to appear near the zone edges of the Fermi surface. The persistence of the zone-center hole pocket and the appearance of these large electron pockets under pressure explain the persistent multiband behavior as well as the change in sign of  $\rho_{xy}$ .

The pressure-dependent evolution of the structure and electrical transport of  $\text{Bi}_4\text{Te}_3$  is summarized in Fig. 3. Near 6 GPa,  $\text{Bi}_4\text{Te}_3$  transforms from its ambient-pressure,  $R\bar{3}m$  structure into a monoclinic  $C2/m$  structure similar to elemental Bi.<sup>12</sup> Concomitant with this structural transformation is the reduction in the value of  $\rho(10 \text{ K})$  and a change in the sign of the Hall coefficient,  $R_H$ . Superconductivity develops out of this  $\text{Bi}_4\text{Te}_3$ -II phase, but with a relatively low critical temperature of  $T_c = 2.1 \text{ K}$  at 8.2 GPa. Increasing pressure compresses the monoclinic structure, which exhibits only a slightly stiffer lattice than the  $\text{Bi}_4\text{Te}_3$ -I phase. With the lattice compression from 6 to 12 GPa, superconductivity is enhanced, reaching  $T_c = 3.7 \text{ K}$  at 12.8 GPa.

Applying further pressure instigates the ingrowth of the bcc phase of  $\text{Bi}_4\text{Te}_3$ -IV, which manifests a new superconducting state with a  $T_c$  greater than twice that of the maximum  $T_c$  observed in the  $\text{Bi}_4\text{Te}_3$ -II phase. With increasing pressure,

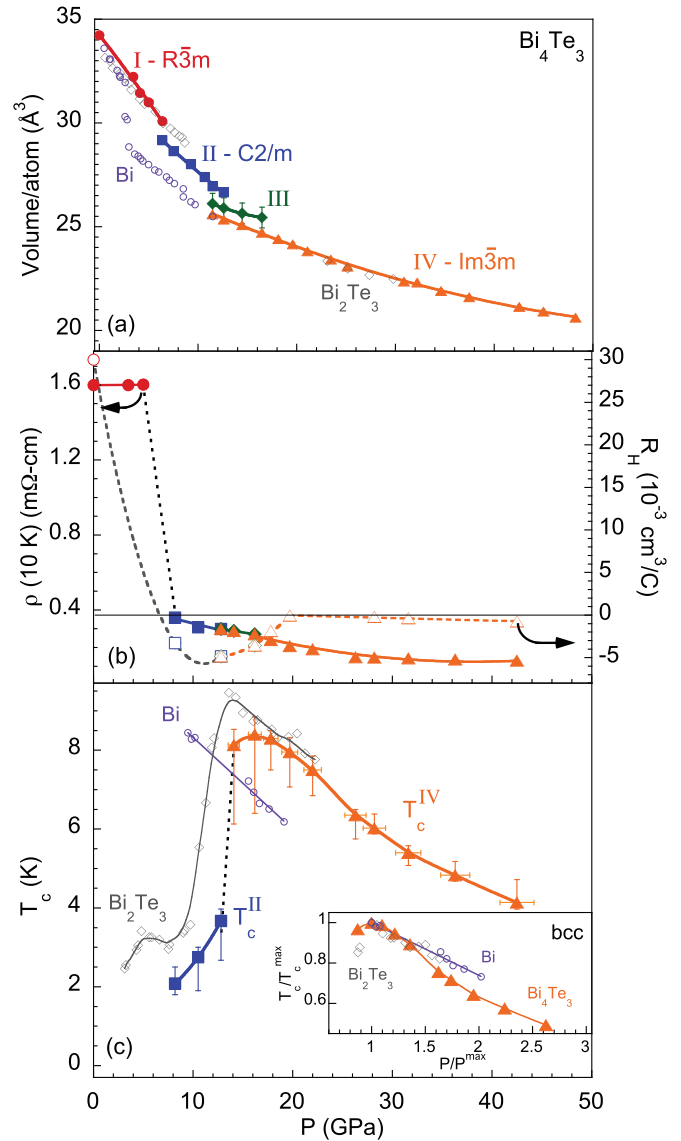


FIG. 3. (Color online) Pressure-dependent evolution of the structural and electronic properties of  $\text{Bi}_4\text{Te}_3$ . (a) The equation of state (volume/atom) of  $\text{Bi}_4\text{Te}_3$  reveals three pressure-induced structural transformations; data for Bi (Ref. 12; open, purple circles) and  $\text{Bi}_2\text{Te}_3$  (Ref. 14; open, gray diamonds) are included. (b) The electrical resistivity at 10 K,  $\rho$  (10 K) (closed symbols, left axis) and the Hall coefficient,  $R_H$  (open symbols, right axis) suggest metallization under pressure. (c) The evolution of superconductivity under pressure reveals a maximum  $T_c = 8.4 \text{ K}$  near 16.2 GPa, within the bcc phase. Vertical error bars represent widths of the superconducting transitions, while horizontal error bars represent uncertainty in pressure. Data for Bi (Ref. 15) and  $\text{Bi}_2\text{Te}_3$  (Ref. 17) under pressure are included (open symbols) for comparison. Inset: scaled evolution of  $T_c/T_c^{\text{max}}$  versus  $P/P^{\text{max}}$  in the bcc phases of  $\text{Bi}_4\text{Te}_3$ ,  $\text{Bi}_2\text{Te}_3$ , and Bi. In all cases, solid and dashed lines are guides to the eye.

$\text{Bi}_4\text{Te}_3$  transforms completely to the bcc phase and  $|R_H|$  reaches a minimum, indicating a high-carrier-density metallic phase.  $T_c$  reaches a maximum value of 8.4 K at 16.2 GPa. Pressures above 20 GPa result in an increase in  $|R_H|$ —corresponding to a decrease in the carrier concentration—and a simultaneous suppression of  $T_c$ . The simultaneous occurrence of a high-carrier-density metal and a maximum in  $T_c$  upon

entering into a bcc crystal structure is also evident in Bi and  $\text{Bi}_2\text{Te}_3$ .<sup>15,17</sup> Indeed, the pressure-dependent evolution of  $T_c$  in the bcc phases of  $\text{Bi}_4\text{Te}_3$ ,  $\text{Bi}_2\text{Te}_3$ , and Bi are strikingly similar [inset Fig. 3(c)].

In summary,  $\text{Bi}_4\text{Te}_3$  displays two distinct superconducting states arising from different high-pressure structural modifications: monoclinic  $\text{Bi}_4\text{Te}_3$ -II, a low-carrier-density multiband metal; and bcc  $\text{Bi}_4\text{Te}_3$ -IV, which displays archetypal metallic behavior. The striking similarities between the pressure-dependent structures and evolutions of  $T_c$  in the bcc phases of Bi,  $\text{Bi}_2\text{Te}_3$ , and  $\text{Bi}_4\text{Te}_3$  hint at universal behavior manifesting under pressure within the  $(\text{Bi}_2)_m(\text{Bi}_2\text{Te}_3)_n$  series. Understanding how the disparate ambient-pressure states of the  $(\text{Bi}_2)_m(\text{Bi}_2\text{Te}_3)_n$  series ultimately converge to this universal high-pressure behavior could provide insights into the conditions favoring topological insulators and superconductors.

We thank K. Visbeck, J. Park-Klepeis, and C. Kenny-Benson for assistance and beamline support. Portions of this

work were performed under LDRD. Lawrence Livermore National Laboratory is operated by Lawrence Livermore National Security, LLC, for the US Department of Energy (DOE), National Nuclear Security Administration (NNSA), under Contract No. DE-AC52-07NA27344. Portions of this work were performed at HPCAT (Sector 16), Advanced Photon Source (APS), Argonne National Laboratory. HPCAT is supported by CIW, CDAC, UNLV, and LLNL through funding from DOE-NNSA, DOE-BES, and NSF. Use of the APS, an Office of Science User Facility operated for the US DOE Office of Science by Argonne National Laboratory, was supported by the US DOE under Contract No. DE-AC02-06CH11357. Beamtime was provided through the General User Proposal program. Sandia is a multiprogram laboratory operated by Sandia Corporation, a Lockheed Martin Company, for the US DOE NNSA under Contract No. DE-AC04-94AL85000. Work at Sandia was supported by the LDRD program. Y.K.V. acknowledges support from DOE-NNSA Grant No. DE-FG52-10NA29660.

- <sup>1</sup>L. Fu and C. L. Kane, *Phys. Rev. Lett.* **100**, 096407 (2008).
- <sup>2</sup>J. D. Sau, R. M. Lutchyn, S. Tewari, and S. Das Sarma, *Phys. Rev. B* **82**, 094522 (2010).
- <sup>3</sup>L. Hao and T. K. Lee, *Phys. Rev. B* **83**, 134516 (2011).
- <sup>4</sup>X.-L. Qi, T. L. Hughes, S. Raghu, and S.-C. Zhang, *Phys. Rev. Lett.* **102**, 187001 (2009).
- <sup>5</sup>Y. S. Hor, A. J. Williams, J. G. Checkelsky, P. Roushan, J. Seo, Q. Xu, H. W. Zandbergen, A. Yazdani, N. P. Ong, and R. J. Cava, *Phys. Rev. Lett.* **104**, 057001 (2010).
- <sup>6</sup>L. Fu and E. Berg, *Phys. Rev. Lett.* **105**, 097001 (2010).
- <sup>7</sup>J. L. Zhang, S. J. Zhang, H. M. Weng, W. Zhang, L. X. Yang, Q. Q. Liu, S. M. Feng, X. C. Wang, R. C. Yu, L. Z. Cao, L. Wang, W. G. Yang, H. Z. Liu, W. Y. Zhao, S. C. Zhang, X. Dai, Z. Fang, and C. Q. Jin, *Proc. Natl. Acad. Sci.* **108**, 24 (2011).
- <sup>8</sup>J. W. G. Bos, H. W. Zandbergen, M.-H. Lee, N. P. Ong, and R. J. Cava, *Phys. Rev. B* **75**, 195203 (2007).
- <sup>9</sup>D. Hsieh, Y. Xia, L. Wray, D. Qian, A. Pal, J. H. Dil, J. Osterwalder, F. Meier, G. Bihlmayer, C. L. Kane, Y. S. Hor, and R. J. Cava, *Science* **323**, 919 (2009).
- <sup>10</sup>P. Roushan, J. Seo, C. V. Parker, Y. S. Hor, D. Hsieh, D. Qian, A. Richardella, M. Z. Hasan, R. J. Cava, and A. Yazdani, *Nature (London)* **460**, 1106 (2009).
- <sup>11</sup>Y. L. Chen, J. G. Analytis, J.-H. Chu, Z. K. Liu, S.-K. Mo, X. L. Qi, H. J. Zhang, D. H. Lu, X. Dai, Z. Fang, S.-C. Zhang, I. R. Fisher, Z. Hussain, and Z.-X. Shen, *Science* **325**, 178 (2009).
- <sup>12</sup>O. Degtyareva, M. I. McMahon, and R. J. Nelmes, *High Press. Res.* **24**, 319 (2004).
- <sup>13</sup>A. Nakayama, M. Einaga, Y. Tanabe, S. Nakano, F. Ishikawa, and Y. Yamada, *High Press. Res.* **29**, 245 (2009).
- <sup>14</sup>M. Einaga, A. Ohmura, A. Nakayama, F. Ishikawa, Y. Yamada, and S. Nakano, *Phys. Rev. B* **83**, 092102 (2011).
- <sup>15</sup>M. A. Il'ina and E. S. Itskevich, *Sov. Phys. JETP Lett.* **11**, 218 (1970).
- <sup>16</sup>M. A. Il'ina and E. S. Itskevich, *Sov. Phys. Solid State* **13**, 2098 (1972); **17**, 154 (1975).
- <sup>17</sup>C. Zhang, L. Sun, Z. Chen, X. Zhou, Q. Wu, W. Yi, J. Guo, X. Dong, and Z. Zhao, *Phys. Rev. B* **83**, 140504(R) (2011).
- <sup>18</sup>S. T. Weir, J. Akella, C. Aracne-Ruddle, Y. Vohra, and S. A. Catledge, *Appl. Phys. Lett.* **77**, 3400 (2000).
- <sup>19</sup>D. D. Jackson, J. R. Jeffries, W. Qiu, J. D. Griffith, S. McCall, C. Aracne, M. Fluss, M. B. Maple, S. T. Weir, and Y. K. Vohra, *Phys. Rev. B* **74**, 174401 (2006).
- <sup>20</sup>H. K. Mao, J. Xu, and P. M. Bell, *J. Geophys. Res.* **91**, 4673 (1986).
- <sup>21</sup>W. L. Vos and J. A. Schouten, *J. Appl. Phys.* **69**, 6744 (1991).
- <sup>22</sup>A. Hammersley, S. Svensson, M. Hanfland, A. Fitch, and D. Hausermann, *High Press. Res.* **14**, 235 (1996).
- <sup>23</sup>A. C. Larson and R. B. Von Dreele, Los Alamos National Laboratory Report LAUR 86-748 (1994).
- <sup>24</sup>B. H. Toby, *J. Appl. Crystallogr.* **34**, 210 (2001).
- <sup>25</sup>P. Giannozzi *et al.*, [<http://www.quantum-espresso.org>].
- <sup>26</sup>W. Kohn and L. J. Sham, *Phys. Rev.* **140**, A1133 (1965).
- <sup>27</sup>R. M. Brugger, R. B. Bennion, and T. G. Walton, *Phys. Lett. A* **24**, 714 (1967).
- <sup>28</sup>See Supplemental Material at <http://link.aps.org/supplemental/10.1103/PhysRevB.84.092505> for a description of the semimetal behavior of  $\text{Bi}_4\text{Te}_3$  under ambient conditions.